Cement and Concrete Research 142 (2021) 106356

Contents lists available at ScienceDirect

Cement and Concrete Research

journal homepage: www.elsevier.com/locate/cemconres

Normal and anomalous self-healing mechanism of crystalline calcium silicate hydrates

Romain Dupuis [a,1], Juhyuk Moon [b,*,1], Yeonung Jeong [c], Rae Taylor [d], Sung-Hoon Kang [b], Hegoi Manzano [e], Andrés Ayuela [f], Paulo J.M. Monteiro [d,*], Jorge S. Dolado [f]

[a] CNRS/MIT/AMU Joint Laboratory MultiScale Materials Science for Energy and Environment, UMI <MSE>2, Massachusetts Institute of Technology, 77 Massachusetts Avenue, Cambridge, MA 02139, USA
[b] Department of Civil and Environmental Engineering, Institute of Construction and Environmental Engineering, Seoul National University (SNU), 1 Gwanak-ro Gwanak gu, Seoul 08826, Republic of Korea
[c] Construction Technology Research Center, Korea Conformity Laboratories (KCL), 199 Gasan digital 1-ro Geumcheon-gu, Seoul 08503, Republic of Korea
[d] Department of Civil and Environmental Engineering, University of California, Berkeley, CA 94720, USA
[e] Department of Physics, University of the Basque Country UPV/EHU, Barrio Sarriena s/n, 48940, Leioa, Bizkaia, Spain
[f] DIPC and CFM-MPC CSIC-UPV/EHU, p. Manuel de Lardizabal 4, 20018 Donostia-San Sebastián, Spain

ARTICLE INFO

Keywords:
Calcium silicate hydrate
Cement hydrate
Tobermorite
Self-healing mechanism
Molecular simulation

ABSTRACT

The origin of different stability of crystalline calcium silicate hydrates was investigated. The tobermorite crystal has been used as an analog of cement hydrate that is being mostly manufactured material on earth. Normal tobermorite is thermally unstable and transforms to amorphous at low pressure. Meanwhile, anomalous tobermorite with high Al content does not significantly transform under high pressure or high temperature. Conducted X-ray absorption spectroscopy explains the weak stability of normal tobermorite which was originally hypothesized by the role of zeolitic Ca ions in the cavities of silicate chains. Atomic simulations reproduced the experimentally observed trend of pressure behavior once the ideal structures were modified to account for the Al content as well as the chain defects. The simulations also suggested that the stability of tobermorite under stress could be rationalized as a self-healing mechanism in which the structural instabilities were accommodated by a global sliding of the CaO layer.

1. Introduction

Silicates are globally formed in nature and are among the most manufactured materials [1], and they can be structured as well-ordered crystals or amorphous glass. Each of these structures have different applications, such as the silicate glasses used for radioactive material storage [2], the silicate crystals used as cation exchangers for various waste encapsulation purposes [3], and the silicates with cavities used for their capacity to store water, with prospective application for energy storage. The silicate minerals present different phases depending on their composition and polymerization order. As an example, tobermorite mineral group comprises several layered calcium silicate hydrates with similar structures but with different degrees of hydration and compositions at the interlayers (Table S1). Tobermorite has been extensively studied for its close structural analogy with calcium (alumino) silicate hydrate (C-[A]-S-H) gel [4], the main hydration product of ordinary Portland cement [5–8] as well as the role of the main binding phase in ancient Roman concrete [9,10]. Since the C-S-H gel is a poorly crystalline phase, the Ca/Si ratio is frequently used to characterize the structure of the gel. For example, the Ca/Si ratios of C-S-H gel normally varies in the range 1.7–1.9 that can be reduced to 1.4–1.6 with the use of supplementary cementitious materials [11,12]. In addition, due to the presence of interlayer in C-S-H, cross-linked silicate tetrahedra (Q^3) is not typically observed in cementitious system [13]. Nevertheless, the crystalline tobermorite is actively being used to simulate realistic models of C-(A)-S-H gel in cement hydrate [5,6,8,14–16]. Therefore, understanding phase transitions and thermodynamic stability of the tobermorite under pressure or temperature is crucial for stabilizing silicate-based materials, investigating Earth's minerals, elucidating failure mechanism of cement-based materials, and developing high

* Corresponding authors.
E-mail addresses: juhyukmoon@snu.ac.kr (J. Moon), monteiro@ce.berkeley.edu (P.J.M. Monteiro).
[1] These authors contributed equally.

https://doi.org/10.1016/j.cemconres.2021.106356
Received 30 November 2019; Received in revised form 26 December 2020; Accepted 31 December 2020
Available online 19 January 2021

resistant cement-based composites.

Tobermorites exist in three hydration states: tobermorite 14 Å (plombierite, $Ca_5Si_6O_{16}[OH]_2$ $7H_2O$) [17], tobermorite 11 Å (tobermorite, $Ca_5Si_6O_{16}[OH]_2$ $5H_2O$) [18], and tobermorite 9 Å (riversideite, $Ca_5Si_6O_{16}[OH]_2$) [19]. The notations 14 Å, 11 Å, and 9 Å refer to the size of basal spacing between consecutive CaO layers. The structure commonly found under ambient conditions is tobermorite 11 Å or 14 Å, which usually transforms tobermorite 9 Å (the so-called normal tobermorite) upon heating to 300 °C. However, some varieties of tobermorite 11 Å do not shrink to 9 Å upon heating; these are known as anomalous tobermorite.

The origin of the dissimilar thermal stabilities of normal and anomalous tobermorite has been the subject of many experimental works, and different explanations have been sought in terms of structural differences. The first structural models were proposed by Megaw and Kelsey [1] and Hamid [20]. However, the currently accepted model of tobermorite 11 Å was theorized by Merlino et al. [18,21]. This model rationalizes the structure of tobermorite in terms of CaO layers sandwiched by infinite wollastonite-type silicate chains, which form zeolitic cavities by establishing links with the adjacent silicate chains. According to this structural model, the most distinctive feature of the normal and anomalous varieties of tobermorite relies on the presence or absence of zeolitic calcium cations in the cavities. The model thus proposes the ideal compositions of $Ca_4Si_6O_{15}(OH)5H_2O$ and $Ca_{4.5}Si_6O_{16}(OH)_25H_2O$ for the normal and anomalous varieties, respectively. According to this structural hypothesis, the zeolitic Ca cations of normal tobermorite are coordinated to oxygen atoms from the silicate chains and from water molecules. Thus, when water molecules leave the zeolitic cavities during heating, Ca ions can only coordinate to silicate chain oxygen, and the generated electrostatic forces are adequate to depolymerize the bridging sites and bring the layer collapse, reaching the equilibrium distance at about 9 Å. In anomalous tobermorite, however, no zeolitic Ca cations exist in the cavities; consequently, proper calcium re-coordination does not occur by dehydration (i.e., no severe structural rearrangement occurs).

The above structural picture based on the role of zeolitic Ca cations seems to provide a reasonable justification for the different thermal behaviors of normal and anomalous tobermorite. However, a detailed explanation for the mechanisms controlling the structural rearrangement, as well as any experimental evidence to prove the presence of zeolitic Ca cations, is still missing. Recently, the crystallographic and spectroscopic studies of Biagioni et al. [22] have provided new clues in this respect. According to these authors, the heating process induces a topotactic transformation that comprises an amorphization with the appearance of both clinotobermorite-like configurations and an intermediate phase with a basal distance about 10 Å prior to the break of the Si-O-Si bond and formation of tobermorite 9 Å. During this transformation, bridging SiO_4 tetrahedra are tilted in a xonotlite-like configuration [22]. The proposed mechanism should depend on the local environment of the bridging sites, so a priori might explain why aspects like the polymerization degree [23] or the incorporation of aluminum [24] have been known to affect the thermal behavior of tobermorite.

Since the debate about tobermorite's stability is still unsettled, any hint on its structure provided by advanced experimental or numerical simulation techniques would be tremendously beneficial. So far, most of these studies have focused on structural details over perfected [25] or defected [26,27] tobermorites, disregarding the discussion about the kinetic mechanisms governing the stability of tobermorite or interplay among aluminum substitution, broken silicate chain, and zeolitic Ca ion. In fact, most of the experimental and computational difficulties in assessing the structural differences between normal and anomalous tobermorite 11 Å with respect to thermal stability seem to rest on the concurrent loss of water. Furthermore, the attempts to establish the comparison to the thermal stability experiments have been largely impeded by the inherent stoichiometry variations in naturally found minerals or during the thermal treatments.

Here, synchrotron-based extended x-ray absorption fine structure (EXAFS) and high-pressure x-ray diffraction (HPXRD) experiments over normal and anomalous tobermorite samples are presented. These experiments provided a novel perspective for understanding the atomic scale local environment and the stability of tobermorite. Furthermore, ^{29}Si magic angle spinning nuclear magnetic resonance (NMR) experiments and molecular dynamics (MD) simulations were combined to establish appropriate structure-performance relationships. New atomic insights were given on the mechanism proposed as controlling the local distortion of the bridging sites. This mechanism appeared to be a self-healing mechanism that was perfect in the case of anomalous varieties and imperfect in the case of normal tobermorite.

2. Materials and methods

2.1. Materials and thermal treatment

The impact of a thermal treatment was studied over one anomalous tobermorite 11 Å specimen obtained from Mine Lac d'Amiante, Quebec, Canada, and one normal tobermorite 14 Å specimen from Crestmore, California, US [17]. In ex-situ XRD study, the samples were vacuum-heated at each targeted temperature (125, 135, 150, 180, 300, 330, and 400 °C) for 24 h, and then an x-ray with a wavelength of 0.6199 Å was exposed to the samples for 10 min. As explained later, normal tobermorite 11 Å was obtained by heating the normal tobermorite 14 Å at 135 °C for 24 h (Fig. 1). Therefore, subsequent experiments have been conducted on the obtained normal tobermorite 11 Å.

2.2. Extended X-ray absorption fine structure (EXAFS)

Ca K-edge X-ray absorption spectra (3950 to 4700 eV) of normal and anomalous 11 Å tobermorites were scanned at ambient temperature, using an X-ray absorption fine structure for catalysis (XAFCA) beamline facility at Singapore Synchrotron Light Source (SSLS), Singapore [28]. Two tobermorite 11 Å crystals were finely ground with boron nitride (BN) and were pelletized for the experiment in a transition mode. The absorption spectra were collected three times and averaged to reduce the noise signal of the measured data. Athena software [29] was utilized for the data processing of the normalization of collected spectra, data conversion from energy (eV) to wave vector (k), and computation of Fourier transform, using Hanning window function over a k range of 3 11 0.5 (Fig. 1). Artemis software [29] was used to fit experimental and theoretical absorption threshold. To calculate theoretical distances of Ca-x, where x is O, Si, or Ca, ab initio code of FEFF-6 [30] was utilized based on Merlinos 11 Å tobermorite model [18]. Among the fitting parameters, the many-body amplitude reduction factor i.e., S_0^2 was fixed as 0.982, as a result of fitting a reference material of $Ca(OH)_2$, where coordination number (CN) and radial distance (R) were fixed with the crystallographic data of portlandite and the Debye-Waller factor ($_i$) of Ca—O1 (first shell) and S_0^2 were fitted with varying k-weight factors, k = 1–3. For the analysis of tobermorite data, only one shell per one element was considered. Processed radial distribution plots with fitted data are presented in Fig. S2.

2.3. Nuclear magnetic resonance (NMR)

For ^{29}Si MAS NMR measurements, the two tobermorite 11 Å samples were finely ground and packed evenly into 3.6 mm zirconia rotor and sealed at the open end with a Vespel cap. The rotor was spun at 20 kHz on a Bruker Ultrashild 600WB Plus with a 14.1 T magnet, operating at 119.23 MHz. The magic angle was set to 54.734°, using KBr as a reference. The relatively high spinning speed combining with the high magnetic field was chosen, to provide an increased resolution. Deconvolution of the spectra was performed, assuming a voigt line shape and no loss of information to spinning side bands. In order to quantify the

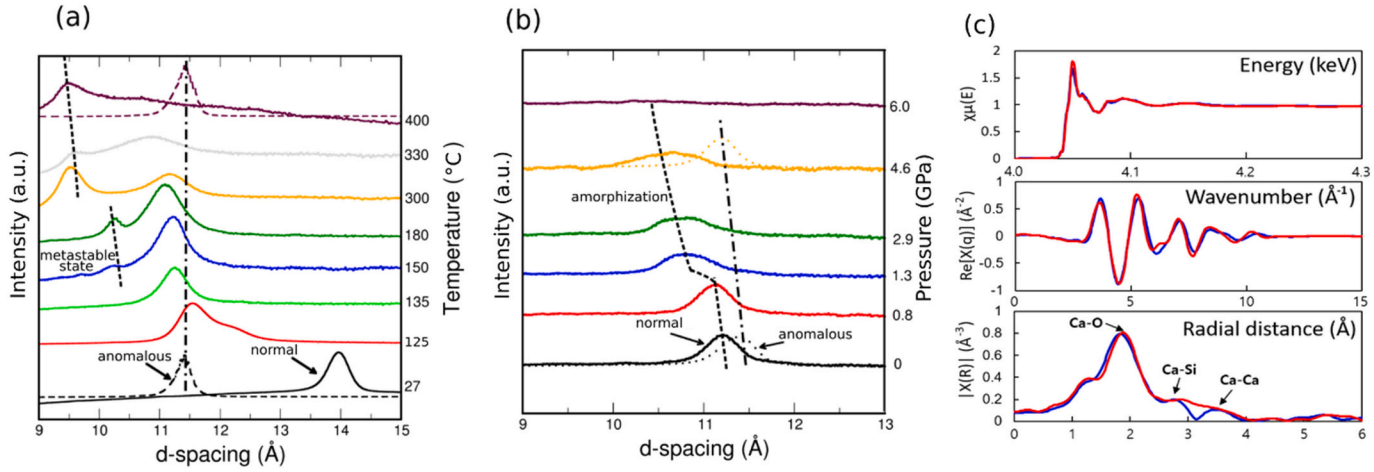

Fig. 1. Variation of layer thickness under heating (a) and pressure (b) explained by Ca-EXAFS experimental result (c). Stepwise dehydration resulted in subsequent contractions of the interlayer in normal tobermorite, while no contraction occurred in anomalous tobermorite. This different thermal response was previously hypothesized as due to the role of zeolitic Ca ions in cavities of normal tobermorite but has not yet been experimentally verified. For the first time, this study experimentally computed the radial distance and coordination number of Ca ions in two tobermorite crystals. (a) Basal peak trajectories for different temperatures ranging from 300 K to 600 K. The patterns for anomalous tobermorite are given in dotted lines for comparison. (b) Basal peak trajectories for different pressures ranging from 0 GPa to 6 GPa. (c) The larger coordination number of Ca—Ca bond in normal tobermorite (3.05 in blue line) compared to that in anomalous tobermorite (2.93 in red line) indicated the existence of additional Ca ion, possibly in the cavities of the silicate chain. This might support the previous hypothesis explaining the different thermal stabilities proposed by Merlino et al. [8]. (For interpretation of the references to color in this figure legend, the reader is referred to the web version of this article.)

information, the different tetrahedral environments are designated Q^n, where Q is a silicate tetrahedron and n denotes the connectivity of the silicate tetrahedron via oxygen, therefore limiting n to the valence of oxygen. By defining the environment there was the possibility of defined separated ranges of chemical shifts [31]. Q^0 represents isolated tetrahedral in the range of −66 to −74 ppm. Q^1 represents chain-end group tetrahedra which can be also considered as half a dimer, with a typical chemical shift at around −77 to −82 ppm. Q^2 represents middle-chain groups where both adjacent tetrahedra are occupied by silicon with a silicon with a shift at around −85 to −89 ppm. Other middle-chain groups occur from substitution of silicon tetrahedra with aluminum tetrahedra. These are represented by Q^n(mAl) [32] where the silicate tetrahedra are connected via n bridging oxygen to mAl; m being the number aluminum ions substituted and n-m other silicate atoms. The most common Q^n(mAl) found in cement is Q^2(1Al); this represents middle-chain groups where one of the adjacent tetrahedra is occupied by aluminum, resulting in a down-field shift of around 3 ppm, giving a typical value of −82 ppm. This shift is called deshielding as it is the result of removal of electron density, magnetic induction, or other effects, which effectively forms a barrier around the nucleus of inner shell electrons, decreasing the pull of outer shell electrons. Q^3 represents branching sites and Q^4 cross-linking sites in a three dimensional framework in the ranges of −95 to −100 ppm and from 103 to 115 ppm, respectively [23]. Deconvolution data is listed in Table S3.

2.4. High-pressure X-ray diffraction (HPXRD)

The HPXRD experiments for the normal and anomalous tobermorite 11 Å were carried out at the beamline 12.2.2 of the Advanced Light Source [33]. High pressures were generated using a diamond anvil cell. The mineral was finely ground and mixed with a pressure medium and a few chips of ruby a pressure indicator. Samples were placed into a sample chamber within a gasketed diamond anvil cell. The sample chamber size was 180 mm diameter with 75 mm thickness. The sample was equilibrated for about 20 min at each pressure. The same pressure-transmitting medium of 4:1 methanol:ethanol was used for all HPXRD measurements. Exposure times of 600 s were chosen to collect powder diffraction patterns. The pressure was measured at off-line using the ruby fluorescence technique [34]. For anomalous tobermorite 11 Å, x-ray beam of $\lambda = 0.6199$ Å and refined sample-to-detector distance of 221.9 mm were used. In the case of normal tobermorite 11 Å, same wavelength and sample-to-detector distance of 280.6 mm were selected (Fig. S1). For both tobermorite crystals, peak positions based on orthorhombic unit cell with I2mm space group show excellent agreement with those reported by Bonaccorsi et al. [17]. For the crystal structure analysis of anomalous tobermorite 11 Å, diffraction peak positions of (002), (004), (011), (101), (015), (110), (112), (017), (022), (024), (107), (019), (0010), (123), (118), (125), (200), (130) and (217) were used to calculate the orthorhombic unit cell volume of tobermorite 11 Å [17]. In addition, diffraction peak positions of (002), (110), (017), (0010), (127), (130) and (217) were chosen for normal tobermorite 11 Å. Refined lattice parameters under pressures are shown in Tables S4–5 and Figs. S3–4. Lastly, pressure-volume data was used to fit Birch-Murnaghan Equation of State (BM EoS) to compute the isothermal bulk modulus at zero pressure (K_0) [35]. The 2nd order BM EoS fitting results provide K_0 values of 71(4) and 63(2) GPa for normal and anomalous tobermorite 11 Å, respectively (Figs. S5 and S6).

2.5. Molecular dynamics (MD) simulation

The structural response to pressure of normal and anomalous tobermorite models were simulated using Gulp [36] and LAMMPS packages [37]. Forces were evaluated using the ReaxFF [38] force field which is a reactive multi-body potential that reproduces bond breaking or formation. A combination of different parameters was used to simulate the tobermorite with aluminum substitutions that contains Al, Ca, Si, O and H atoms [39–41]. These potentials are well suited empirical force fields available for an analysis of structural changes induced by pressure in tobermorite systems. The initial structures were built according to the NMR signal which are explained in detail in Section 3.5.

3. Results

3.1. Thermal stability

As seen in Fig. 1(a), the ex-situ thermal XRD experiments confirmed

the expected thermal stability of the two tobermorite 11 Å crystals; the basal space did not shrink when the anomalous tobermorite was heated at 300 °C for 24 h. However, Fig. 1(a) illustrates the well-known collapse of the basal peak of tobermorite 14 Å when the tobermorite 11 Å phase starts to form at 125 °C [18]. As temperature increased, the peak became broader, indicating an amorphization phenomenon. Remarkably, an additional peak at basal distances about 10.2 Å became noticeable at 150 °C. This tobermorite 10 Å was noticeable at 180 °C. As expected, the 9.3 Å peak indicating that the formation of tobermorite 9 Å was formed at 300 °C with coexistence of a broad peak around 11 Å. At 400 °C, the 11 Å peak totally disappeared, and only the 9.3 Å peak survived.

3.2. Pressure response

Fig. 1(b) presents HPXRD experiments on the normal and anomalous tobermorite samples performed in the current study. These experiments showed that the dissimilar thermal behaviors of normal and anomalous tobermorite had their analogous behaviors under pressure. The anomalous one exhibited a high structural stability with no significant shrinkage of their basal distance under pressure. Contrarily, normal tobermorite exhibited a progressive amorphization, as reflected by the broadening of the peak. Additionally, crossover behavior occurred at pressures of about 2.5 GPa, the point at which an intermediate phase of tobermorite 10 Å was observed upon heating at 150 °C. The existence of this metastable phase under pressure was unexpected; it could have been related to the dehydration process. The HPXRD experiments seemed to indicate that hydrated tobermorite 10 Å had an energetically unfavorable state at room conditions only if sufficient energy was given. An estimated energy of about 0.06 eV could be given by calculating P (V—V_0) at the crossover pressure; this energy value was well-matched with the thermal energy (3/2kT) at 125 °C. Afterward, the basal spacing of tobermorite 10 Å continued reflecting the progressive amorphization under pressure until it became significantly diffuse around 6 GPa and totally disappeared at 6.3 GPa.

3.3. EXAFS result

To investigate the atomic scale local environment of tobermorites, Ca K-edge EXAFS experiments were performed on normal (i.e., thermally treated tobermorite 14 Å at 135 °C for 24 h) and anomalous tobermorite 11 Å crystals. The convoluted data of radial distance presented almost identical atomic environments of Ca—O (first peak) and Ca—Si (second peak), while a distinct third peak of Ca—Ca was observed in the normal tobermorite 11 Å (Fig. 1[c], Table S2, and Fig. S2). The local environments of Ca—O and Ca—Si were expected to be similar due to the structural arrangement of the main CaO layer and silicate chains in both crystals [18]. The difference of the third peak (i.e., Ca—Ca bond) probably supports the hypothesis of the existence of a zeolitic Ca ion in the cavities of the silicate tetrahedra chain; such an ion would directly increase the average CN of the Ca—Ca bond in the normal tobermorite 11 Å. The fitted CNs for normal and anomalous tobermorites were 3.05 and 2.93, respectively—enough of a difference to support the hypothesis of the existence of zeolitic Ca cations in normal tobermorites. Furthermore, increased averaged radial distance of the Ca—Ca peak in normal tobermorite (3.80 vs. 3.71) also supported this hypothesis although there is still a possibility of Ca presence in other places such as next to the broken silicate chain [12,42]. For instance, a defect of silicate chain may also contribute to a higher CN of the Ca—Ca bond from closer arrangement of interlayer Ca ion to the Ca ion in main layer owing to the negative charge by the defect. For other peaks of Ca—O and Ca—Si bonds, no significant difference in radial distance or CN was found, as summarized in Table S2. Note that the measured bond data in Fig. S2 indicate the length of constructive interference pathway (i.e., distance between the outer surfaces of two atoms) while R values in Table S2 indicate the conventional bond distance between two atoms (i.e., distance between the centers of two atoms).

3.4. NMR result

The observed normal and anomalous behavior of tobermorite under pressure could not be explained in terms of the presence or absence of zeolitic cations, although structural differences have usually been referenced to justify the different thermal responses of the tobermorite varieties. Under pressure, the charge imbalances that take place when water molecules are lost, did not occur. The used pressure-transmitting medium of 4:1 methanol: ethanol mixture might have absorbed water molecules in layered crystals under pressure [43]. However, the amorphization phenomenon was only observed in the normal tobermorite case. Therefore, other structural reasons should be invoked to explain the normal and anomalous characteristics under pressure. The differences might come from the three-dimensional skeleton formed by the (alumino)silicates. In this sense, NMR techniques have proven to be suitable tools to analyze the polymerization of the silicate species as well as Al substation in C-S-H like materials [44–46]. In the NMR technique, Q^n(xAl) nomenclature is generally used for the peaks, where Q^n(xAl) is the chemical shift of a silicon atom that is bound to n tetrahedra by siloxane bonds and x is the number of Al substitutions in these tetrahedra.

Fig. 2(a, c) displays the Si NMR signals measured on normal and anomalous tobermorite. The first feature was the presence of 34% Q^1 sites in normal tobermorite, which indicated a defective silicate chain structure due to missing silicate tetrahedra, which shortened the chains. This Q^1 site was also observed in previous NMR study on naturally found normal tobermorite crystals from Fuka, Okayama, Japan [47]. Experimental [12,48,49] and theoretical [50] evidences have demonstrated that the most favorable site for a vacancy in the chains is the bridging site. Therefore, the absence of silicate tetrahedra in the normal tobermorite implied both shorter chains and the presence of less zeolitic-type cavities or Q^3 sites linking consecutive calcium silicate layers. However, the Q^1 signal in anomalous tobermorite was almost negligible when compared to noise. The relatively short silicate chains in normal tobermorite 11 Å were attributed to the dehydration from tobermorite 14 Å and should have been related to further condensation to tobermorite 9 Å. Both tobermorite 11 Å crystals had a similar Q^3 shift (22–25%), but the anomalous tobermorite 11 Å had a higher Q^2/Q^3 value (3.40) than normal tobermorite (2.01). Thus, it can be concluded that anomalous tobermorite had longer silicate chains, but both samples had a similar amount of branching tetrahedra.

3.5. Structural models for MD simulation

Simulation studies have been performed firstly on two models for normal and anomalous tobermorite as proposed by Merlino et al. [18] that are free from aluminum and composed of infinite chains (denoted as Si-normal and Si-anomalous, respectively). The difference is that Si-normal tobermorite contains Ca^{2+} ions in the interlayer cavities. Thus, the Ca/Si ratio is 0.83 for Si-normal and 0.67 for Si-anomalous. Moreover, two other models, with aluminum substitutions, have been additionally simulated. Starting from the Si-normal and Si-anomalous ideal crystalline structures proposed by Merlino et al., modifications were made based on the ^{29}Si NMR in Fig. 2 (e, f). In essence, the modifications consisted of removing the necessary silicate groups to match the Q^1 percentage in normal tobermorite. While the anomalous model was initially approximated by a perfected structure in which no silicates were removed, 1/3 of the Q^3 sites were substituted by Al, and the generated charge excess was properly compensated by Ca^{2+}. The substitutions of silicon by aluminum have been applied in some bridging sites to match the Al/Si and the Q^3(1Al)/Q^3 ratios for both normal and anomalous tobermorite. Each substitution implied a − 1 charge excess that was compensated by using two different schemes, with 1/2 Ca^{2+} cations placed in the interlayer space or in a single proton. As a result, Al-substituted normal (Al-normal) and anomalous (Al-anomalous) tobermorite 11 Å were constructed, as shown in Fig. 2(b, d). In

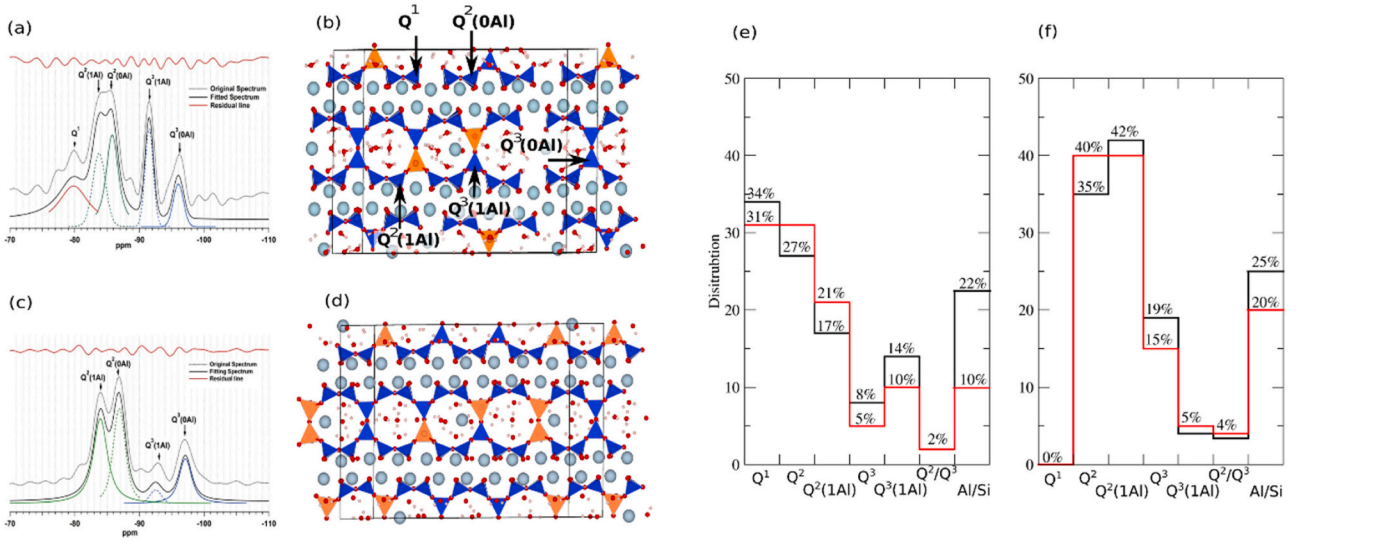

Fig. 2. Al incorporation in silicate chains. (a) NMR signal measured on normal tobermorite and (b) corresponding Al-normal model. (c) NMR signal measured on anomalous tobermorite and (d) corresponding Al-anomalous model. Ca, O, and H atoms are represented in light blue, red, and grey, respectively. SiO_4 and AlO_4 tetrahedra are represented in blue and orange, respectively. Distribution of Q_n extracted from the NMR signals (shown in black line) and corresponding distribution in MD model (shown in red line) for (e) normal and (f) anomalous tobermorite models. (For interpretation of the references to color in this figure legend, the reader is referred to the web version of this article.)

summary, the main difference between Al-normal and Al-anomalous tobermorite is the regular and infinite formation of cavities in anomalous tobermorite in contrast to the vacancies in normal tobermorite that made the links between adjacent layers sparse. The resulting Ca/Si ratio of Al-normal and Al-anomalous is 0.86 and 0.71, respectively. The Al/Si ratio is 0.1 and 0.25 for Al-normal and Al-anomalous models, respectively.

4. Discussion

4.1. Elemental composition and Al substitution

Both of scanning electron microscope – energy dispersive spectrum (SEM-EDS) composition analysis and x-ray fluorescence (XRF) measurement indicated that aluminum content was very low (i.e., Al_2O_3 content was less than 1%) in normal tobermorite which was consistent with previously published elemental composition in two naturally found normal tobermorite crystals [51]. The Al/Si ratio content in anomalous tobermorite was 0.17. Ca/Si ratios of normal and anomalous tobermorite are 1.19 and 0.83, respectively. The slightly higher Ca/Si ratio in normal tobermorite agrees well with the previous studies and EXAFS result (i.e., higher CN of Ca—Ca bond) conducted herein [51]. However, the Si NMR signals (Fig. 2) seemingly indicated the presence of Al in both tobermorites. The plausible explanation on the discrepancy on the Al content in the normal tobermorite is the heterogeneous nature of the naturally collected sample. The Al substitution may occur locally in micro-scale so the required amount for NMR experiment (i.e., less than 100 mg) may not be enough to obtain the representative Al substitution rate from a single NMR experiment. For instance, Maeshima et al. collected natural tobermorite and found a mixture of tobermorite 14 Å and 11 Å in nature and reported the variation of Al/(Al + Si) ratio ranging from 0.02 to 0.13 depending on the location in the crystal [47]. Therefore, it has to be stated that the elemental composition measured from SEM-EDS can be more representative as it was averaged from 10 spot analyses from around 2 g of samples. Also, the value was consistent with the composition data from XRF. In terms of potential sites for Al substitution in tobermorite crystal, Komarneni and Tsuji [3] reported that Al preferably substituted at the chain middle group SiO_4 by ^{29}Si NMR measurements [52]. In contrast, Sasaki et al. [53] reported that the Al substitution occurred at the bridging SiO_4. From the Q^n ratios obtained by the ^{29}Si NMR, and assuming that Al is preferentially located in the bridging sites [31,54–56], an Al/Si ratio of 0.1 and 0.2 could be determined for normal and anomalous tobermorites, respectively. It is widely accepted that aluminum induces polymerization of larger (alumino)silicate chains [31,54–57]; therefore, the lack of Q^1 sites was not surprising. In contrast to the normal form, all possible Q^3 sites in anomalous tobermorite were occupied, forming regular linkages or zeolitic cavities between different layers. If the Lowenstein rule were fulfilled (i.e., Al does not occupy consecutive tetrahedra below 0.5 Al/Si ratio), the amount of Al in anomalous tobermorite should have been larger than necessary to saturate all the bridging sites (0.2). However, violations of the Lowenstein rule have been documented in micas [58] and calcium aluminosilicates [59] when the Al content is adequately high. In addition, phases like tricalcium aluminate indicate that Al-O-Al tetrahedral bonds are possible from a thermodynamic point of view. For example, the Lowenstein rule might be circumvented under some kinetic constraints. For tobermorite 11 Å, the presence of 2 aluminum tetrahedra together in Q^3 bridging sites might be considered a direct consequence of the phase transition from an Al-tobermorite 14 Å. In the latter, the maximum Al/Si ratio could reach 0.5 if all the bridging sites are occupied. Upon dehydration and shrinkage of such structure, the only choice for bridging sites to polymerize and to form Q^3 sites is through Al-O-Al Q^3 sites.

4.2. Comparison of pressure behavior between experiment and simulation

Fig. 3 shows the measured pressure-volume behavior of tobermorite 11 Å compared with MD simulation results. The experiment shows that normal tobermorite is slightly stiffer than anomalous tobermorite under pressure as the fitted bulk modulus indicated (71 GPa vs. 63 GPa). Similar results were found for Si-normal and Si-anomalous tobermorite models whereas Al-normal model is more compressible than Al-anomalous model (Fig. 3[a]). This observation informed a general sense concerning the effect of Al presence in the inosilicates; the Al—O bond was softer and longer than the Si—O bond, and at the same time, the Al-O-Al angles were more malleable than the Si-O-Si or Si-O-Al bonds [27,60–62]. Therefore, it can be induced from MD result that Al substitution generally increases the compressibility. On the other hand,

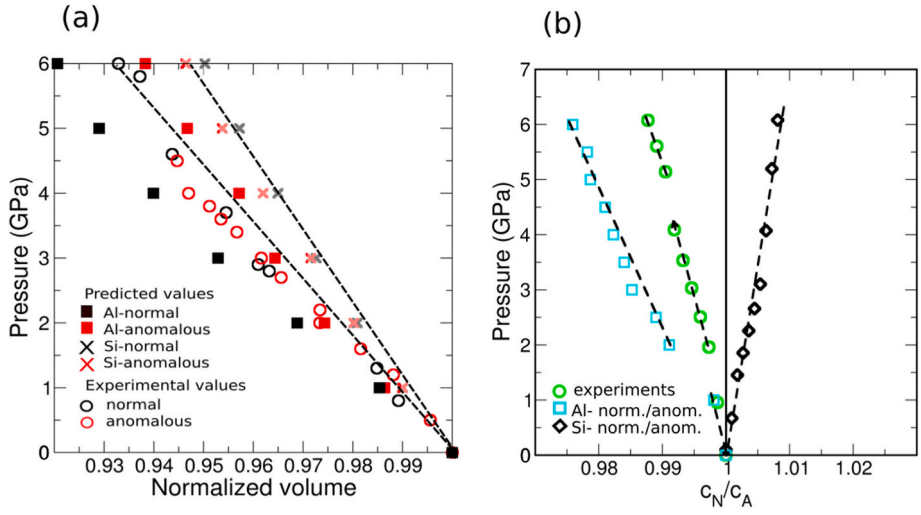

Fig. 3. Pressure induced volume contraction of tobermorite crystals. Experimentally measured (circles) and simulated (lines and crosses) response under pressure: (a) pressure-volume relation and (b) pressure-layer thickness relation. Overall volumetric response appeared similar, whereas layer variation significantly differed depending upon Al substitution and the length of the aluminosilicate chains.

the opposite experimental result was recently reported as Al substituted tobermorite showed higher incompressibility [63]. This was explained by the assumption that Al-induced shorter chain length which might accommodate more charge-balancing Ca and construct a stronger hydrogen bonding system. In our MD study, the other factors of broken silicate chain and zeolitic Ca ion could be controlled. In this environment, the Al substitution increased the compressibility of tobermorite 11 Å.

Additionally, stronger evidence about the pivotal role of addressing structural defects (Al, Q^1 sites, etc.) can be seen in Fig. 3(b), where the evolution of the ratio of the *c*-axis (c_N/c_A) of normal and anomalous tobermorite is displayed as a function of pressure. While the HPXRD experiments (green open circles) and the Al-normal and Al-anomalous models (open squares) showed that the *c*-axis of the normal tobermorite shrunk more than the *c*-axis of the anomalous one, the Si-normal and Si-anomalous models (rhomboid symbols) showed the opposite trend. This contrary behavior indicates that the experimentally observed trend cannot be solely explained by the presence of zeolitic cations which is the main reason of dissimilar thermal behavior hypothesized by Merlino [18,21]. Furthermore, the ratio evolution of c_N/c_A for Al-normal and Al-anomalous (in light blue) indicates that Al-anomalous tobermorite is stiffer than Al-normal tobermorite in the *c*-axis direction.

In summary, the difference between the models for Al-anomalous and Si-anomalous is the presence of aluminum (both systems have infinite chains). We observe that the substitution of Si by Al tends to reduce the stiffness of the material (Fig. 3[a]). This result can be understood by the weaker strength and lower stiffness of Al—O bond [27]. Al-normal, being the most defective system, is also more compressible than Al-anomalous. This is due to the absence of bridges between the silicate chains in the *c*-axis that is the most compressible direction in these systems (see Tables S6 and S7). Finally, in Si-normal and Si-anomalous, the main difference is the presence of interlayer cations in Si-normal and we observe little effect on the compressibility of the system.

4.3. *Self-healing mechanism in Al substituted anomalous tobermorite*

Thermal and pressure-induced transformations of normal tobermorite shared some salient features, such as a progressive amorphization of the structure and the appearance of a metastable phase, like tobermorite 10 Å. As this intermediate phase had the Q^3 sites fully tilted, a key factor controlling the stability of tobermorite was likely its resistance to shear deformations. To investigate this aspect in further detail, the shearing behaviors of all models were simulated. Si-normal shows identical shearing deformation with Si-anomalous (Fig. 4[a]). On the contrary, the other models showed interesting shear behavior due to the either different bond chemistry (Al substitutions) or bonding network (Al-normal has a defective aluminosilicate chain). The deformation was first applied along the direction of the *a*-axis (i.e., creating an angle of 120° with the direction of the chains) with a strain rate of 0.1 ps^{-1}. During the simulation, the silicate chains were dissociated in the Al-normal tobermorite, and the phase started to become disordered. However, the Al-anomalous tobermorite did not have such distortion. Instead, the strain energy was periodically released (Fig. 4[a]) via a sliding mechanism of the silicate chains.

To further analyze this mechanism, the deformation was applied along the direction of the *b*-axis (i.e., the one along the chains) with a strain rate of 0.1 ps^{-1}. The energy variation versus the deformation was calculated and plotted in Fig. 4(b) together with snapshots of the configurations after a shear strain of 0.3 of the simulation box as shown in Fig. 4(c, d). During the first steps of the dynamics (up to a shear strain of 0.18 for Al-normal or 0.21 for Al-anomalous), the energy increased with the deformation. In the dynamics, the interlayer bonds binding the two silicate chains were elongated. Afterward, abrupt drops of the energy were regularly observed when increasing the deformation corresponding to a relaxation of the structure. After relaxation, as shown in Fig. 4 (c), the shape of the cavities of the Al-anomalous model was close to the initial shape, thus reflecting a self-healing mechanism. However, the structure of Al-normal tobermorite (Fig. 4[a, b]) was only partially relaxed.

This finding illustrated that the Al-anomalous tobermorite could accommodate more shear stress than Al-normal tobermorite could. For Al-anomalous tobermorite, the energy returned to zero after each relaxation. The mismatch of the silicate chains (Fig. 4[d]) indicates that tobermorite, without Al substitutions, is more likely to amorphize due to the loss of connectivity in the interlayer region. Fig. 4(b) also shows the energy curve for Si-anomalous model. As can be seen, the energy diverged from the ones of other phases, indicating that this relaxation mechanism was not possible in the samples with full silicon atoms and that the system would continue accumulating energy until the Si-O-Si bond broke.

According to the conducted MD simulations, the self-healing (or self-relaxing) mechanism of the Al-anomalous tobermorite could be ascribed to a global sliding of the CaO layers. The sliding distance is about 1.6 Å,

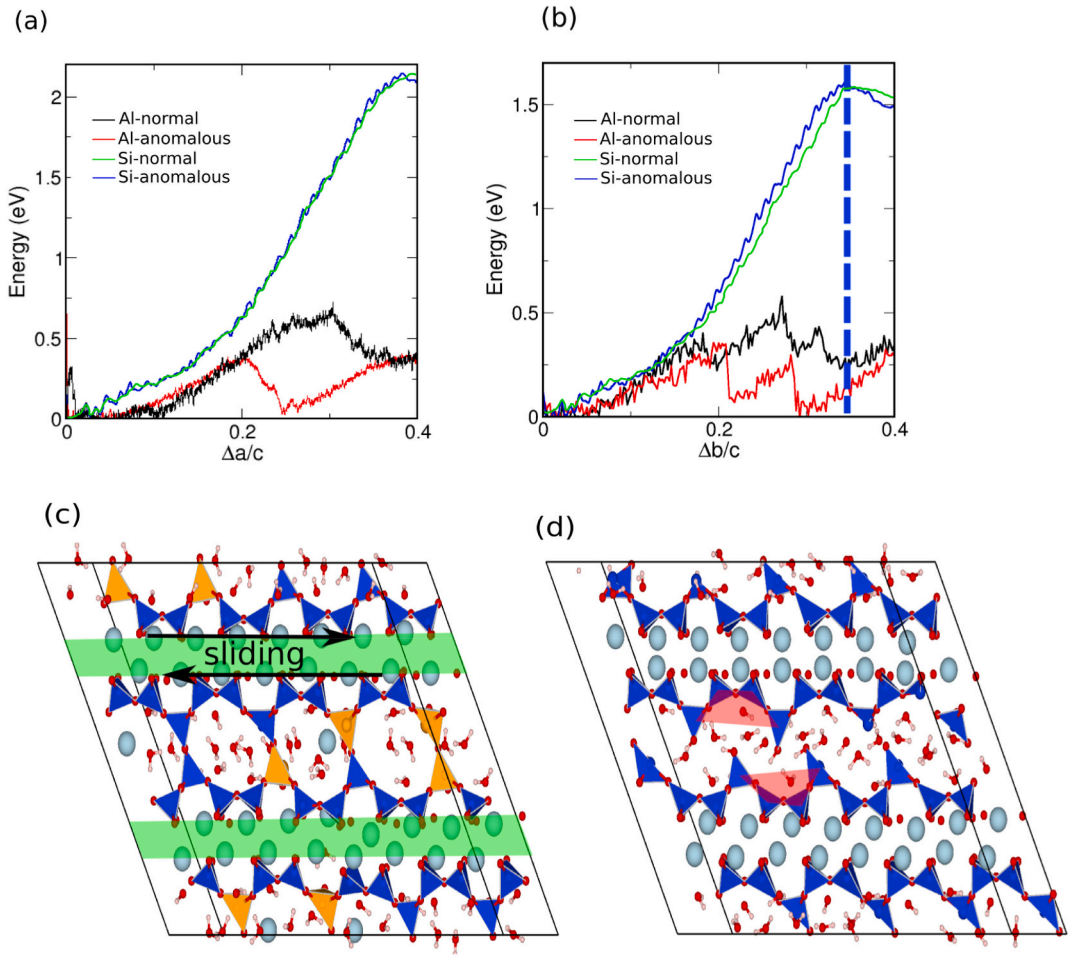

Fig. 4. Different resistant mechanism under shear deformation. Energy versus shear deformation (a) in the *a* direction (Δa/c units) and (b) in the *b* direction (Δb/c units). The snapshots of the different models were plotted at the same stage of deformation of 0.3 for (c) Al-anomalous and (d) Si-anomalous. The role of Al was preserving the links in the double chains; instead, a sliding in the CaO region was observed. The green area indicates the sliding zone that corresponds to the CaO layer in which atoms rearrange during the shear deformation. The red areas were connected at the beginning of the deformation. After breaking the Si-O-Si bridges, there is now a misalignment of the separated silicate chains due to the applied shear stress. (For interpretation of the references to color in this figure legend, the reader is referred to the web version of this article.)

which corresponds to half the Ca—Ca distance (3.85 Å). Thus, for even slides, the alignment is changed compared to the initial one. In this way, the stretching of the Al-O-Al, Al-O-Si, or Si-O-Si bonds was canceled. An atomic local strain analysis [64] measuring the displacement of the atoms compared to their positions in the initial state was performed. This analysis confirmed that the region of main sliding was the CaO layer. In the case of Al-normal tobermorite, this process was observed partially and only for the first relaxation. The presence of previous structural defects (presence of Q^1 sites) made the self-healing mechanism imperfect for this variety, and the system jumped into a structure with more defects upon the sliding of the CaO layers. For Si-anomalous tobermorite, the two chains of silicates were torn apart (Fig. 4[d]) when the deformation reached $\gamma = 0.38$, and the structure relaxed. The energy required for breaking all the bonds was 1.5 eV and corresponded to a chemical reaction in which the Si-O-Si bonds were broken. During the shear simulation, the Al-O-Al, Al-O-Si, or Si-O-Si bonds remained for both Al-normal and Al-anomalous structures. Thus, the energy required to break the bonds was larger than that required for relaxing the structure (about 0.5 eV). However, for the Si-anomalous tobermorite, the Si-O-Si bonds broke before any relaxation of the layers in the CaO region. The longer distance of Al—O bonds compared to Si—O bonds may have favored relaxation in the CaO layer. This finding emphasized that, even if the bulk response to pressure was similar, the presence of aluminum significantly modifies the structural response upon shearing.

5. Conclusion

The key silicate mineral tobermorite is an inosilicate that has been classified into normal and anomalous varieties according to its thermal stability. Herein, synchrotron-based experimental results of extended x-ray absorption fine structure and high pressure x-ray diffraction are presented to elucidate the origin of different thermal stabilities of tobermorite crystals and their responses under pressure, respectively. The anomalous varieties exhibited high structural stability with no significant collapse of the basal space both under pressure and high temperature. Contrarily, normal tobermorite exhibited a progressive amorphization and crossover behavior at pressures of about 2.5 GPa, the point at which an intermediate phase with a basal spacing of 10 Å appeared upon heating at 180 °C.

Different thermal response was previously hypothesized by the role of the zeolitic Ca ion in the cavity of the silicate chains of normal tobermorite. From the conducted x-ray absorption spectroscopy, the coordination number (CN) of the Ca—Ca bond was found to be larger in normal tobermorite (3.05 in normal vs. 2.93 in anomalous); this can help to experimentally support the hypothesis of the presence of an additional zeolitic Ca ion in the cavity of the silicate chains. Also note that additional Ca presence in other positions such as close to the broken silicate chain or interlayer calcium for compensating charge due to Al substitution, is still possible but the other potential locations have not

been proposed to explain the dissimilar thermal behavior of tobermorite. Furthermore, the dissimilar thermal behavior of normal and anomalous tobermorite was related to the pressure-dependent behavior especially as a pressure-induced amorphization. This finding agreed with previous works that emphasized the mapping between the temperature-driven and pressure-driven process [65,66].

Furthermore, ^{29}Si magic angle spinning nuclear magnetic resonance (NMR) experiments and molecular dynamics (MD) simulations were combined to establish appropriate structure-performance relationships. The findings were twofold; on the one hand, the impact of structural defects like Al-substitutions or the presence of shortened chains was crucial to correctly account for the observed behavior of normal and anomalous tobermorite under pressure. On the other hand, new atomic insights were given on the mechanism proposed as controlling the local distortion of the bridging sites. This mechanism appeared to be a self-healing mechanism that was perfect in the case of anomalous varieties and imperfect in the case of normal tobermorite.

Therefore, this study's results provided a new, important step forward in the description of the structure and stability of normal and anomalous tobermorite crystals. Furthermore, these results can be utilized to elucidate failure mechanism of C-S-H like materials, manufacture more heat and pressure-resistant cementitious materials, and stabilize various silicate materials under extreme conditions based on the understanding on the origin of different thermal and pressure resistances from the atomic scale.

CRediT authorship contribution statement

Romain Dupuis: Methodology, Investigation, Data curation, and Writing original draft**. Juhyuk Moon:** Conceptualization, Methodology, Investigation, Data curation, and Writing original draft, Supervision. **Yeonung Jeong:** Investigation, and Data curation. **Rae Taylor:** Investigation, and Data curation. **Sung-Hoon Kang:** Investigation, and Data curation. **Hegoi Manzano:** Validation. **Andrés Ayuela:** Writing-Reviewing and Editing, Supervision. **Paulo J.M. Monteiro:** Conceptualization, Resources, Writing-Reviewing and Editing, Supervision. **Jorge S. Dolado:** Writing-Reviewing and Editing, Supervision

Declaration of competing interest

The authors declare that they have no known competing financial interests or personal relationships that could have appeared to influence the work reported in this paper.

Acknowledgments

J.M. acknowledges support by a grant (20SCIP-C159063-01) from Construction Technology Research Program funded by Ministry of Land, Infrastructure and Transport of Korean government. H.M. acknowledges the financial support from the Gobierno Vasco (project IT912-16). The work in San Sebastián (R.D., J.S.D, A.A) was supported by the Spanish Ministry of Science and Innovation with RTI2018-098554-B-I00, PID2019-105488GB-I00 and PCI2019-103657 research grants, the Gobierno Vasco UPV/EHU (Project No. IT-1246-19), and the European Commission from the NRG-STORAGE project (GA 870114). The Institute of Engineering Research in Seoul National University provided research facilities for this work. The Ca-XAS and HPXRD experiments were performed at XAFCA beamline in Singapore Synchrotron Light Source (SSLS) and 12.2.2 beamline in Advanced Light Source (ALS), respectively. The ALS supported by a DOE Office of Science User Facility under contract no. DE-AC02-05CH11231 and the Consortium for Materials Properties Research in Earth Sciences under NSF Cooperative Agreement EAR 1606856. The authors thank Prof. Simon M. Clark, Dr. Yonghua Du, and Dr. Shibo Xi for helpful discussions and beamline experimental supports.

Appendix A. Supplementary data

Supplementary data to this article can be found online at https://doi.org/10.1016/j.cemconres.2021.106356.

References

[1] H.D. Megaw, C.H. Kelsey, Crystal structure of tobermorite, Nature 177 (1956) 390–391.
[2] J.H. Simmons, P.B. Macedo, A. Barkatt, T.A. Litovitz, Fixation of radioactive waste in high silica glasses, Nature 278 (1979) 729–731.
[3] S. Komarneni, R. Roy, D.M. Roy, C.A. Fyfe, G.J. Kennedy, A.A. Bothner-By, J. Dadok, A.S. Chesnick, ^{27}Al and ^{29}Si magic angle spinning nuclear magnetic resonance spectroscopy of Al-substituted tobermorites, J. Mater. Sci. 20 (1985) 4209–4214.
[4] In cement notation C=CaO, S=SiO_2 and H=H_2O.
[5] A. Kunhi Mohamed, S.C. Parker, P. Bowen, S. Galmarini, An atomistic building block description of C-S-H - towards a realistic C-S-H model, Cem. Concr. Res. 107 (2018) 221–235.
[6] G. Kovačević, B. Persson, L. Nicoleau, A. Nonat, V. Veryazov, Atomistic modeling of crystal structure of Ca1.67SiHx, Cem. Concr. Res. 67 (2015) 197–203.
[7] A.J. Allen, J.J. Thomas, H.M. Jennings, Composition and density of nanoscale calcium–silicate–hydrate in cement, Nat. Mater. 6 (2007) 311–316.
[8] L.B. Skinner, S.R. Chae, C.J. Benmore, H.R. Wenk, P.J.M. Monteiro, Nanostructure of calcium silicate hydrates in cements, Phys. Rev. Lett. 104 (2010) 195502.
[9] M.D. Jackson, S.R. Chae, S.R. Mulcahy, C. Meral, R. Taylor, P. Li, A.-H. Emwas, J. Moon, S. Yoon, G. Vola, H.-R. Wenk, P.J.M. Monteiro, Unlocking the secrets of Al-tobermorite in Roman seawater concrete, Am. Mineral. 98 (2013) 1669–1687.
[10] M.D. Jackson, J. Moon, E. Gotti, R. Taylor, S.R. Chae, M. Kunz, A.-H. Emwas, C. Meral, P. Guttmann, P. Levitz, H.-R. Wenk, P.J.M. Monteiro, Material and elastic properties of Al-tobermorite in ancient roman seawater concrete, J. Am. Ceram. Soc. 96 (2013) 2598–2606.
[11] I.G. Richardson, The nature of C-S-H in hardened cements, Cem. Concr. Res. 29 (1999) 1131–1147.
[12] I.G. Richardson, The calcium silicate hydrates, Cem. Concr. Res. 38 (2008) 137–158.
[13] M. Jung, J.-s. Park, S.-G. Hong, J. Moon, Micro- and meso-structural changes on electrically cured ultra-high performance fiber-reinforced concrete with dispersed carbon nanotubes, Cem. Concr. Res. 137 (2020) 106214.
[14] K.L. Scrivener, P. Juilland, P.J.M. Monteiro, Advances in understanding hydration of Portland cement, Cem. Concr. Res. 78 (2015) 38–56.
[15] M. Bauchy, M.J.A. Qomi, F.-J. Ulm, R.J.-M. Pellenq, Order and disorder in calcium–silicate–hydrate, J. Chem. Phys. 140 (2014) 214503.
[16] R.J.-M. Pellenq, A. Kushima, R. Shahsavari, K.J. Van Vliet, M.J. Buehler, S. Yip, F.-J. Ulm, A realistic molecular model of cement hydrates, PNAS 106 (2009) 16102–16107.
[17] E. Bonaccorsi, S. Merlino, Modular microporous minerals: Cancrinite-davyne group and C-S-H phases, Rev. Mineral. Geochem. 57 (2005) 241–290.
[18] S. Merlino, E. Bonaccorsi, T. Armbruster, The real structure of tobermorite 11A: normal and anomalous forms, OD character and polytypic modifications, Eur. J. Mineral. 13 (2001) 14.
[19] J.D.C. McConnell, The hydrated calcium silicates riversideite, tobermorite, and plombierite, Mineral. Mag. J. Mineral. Soc. 30 (1954) 293–305.
[20] S.A. Hamid, The crystal structure of the 11 Å natural tobermorite $Ca_2{\cdot}25[Si_3O_7{\cdot}5(OH)_{1.5}]{\cdot}1H_2O$, Z. Kristallogr. Cryst. Mater. 154 (1981) 189.
[21] S. Merlino, E. Bonaccorsi, T. Armbruster, The real structures of clinotobermorite and tobermorite 9 Å : OD character, polytypes, and structural relationships, Eur. J. Mineral. 12 (2000) 411–429.
[22] C. Biagioni, S. Merlino, E. Bonaccorsi, The tobermorite supergroup: a new nomenclature, Mineral. Mag. 79 (2015) 485–495.
[23] W. Wieker, A.R. Grimmer, A. Winkler, M. Mägi, M. Tarmak, E. Lippmaa, Solid-state high-resolution ^{29}Si NMR spectroscopy of synthetic 14 Å, 11 Å and 9 Å tobermorites, Cem. Concr. Res. 12 (1982) 333–339.
[24] R. Gabrovšek, B. Kurbus, Z. Lengar, Comparison of unsubstituted and aluminum-containing synthetic tobermorites characterized by different methods, Cem. Concr. Res. 16 (1986) 325–332.
[25] R. Dupuis, J.S. Dolado, J. Surga, A. Ayuela, Tracing polymerization in calcium silicate hydrates using Si isotopic fractionation, J. Phys. Chem. C 122 (2018) 8356–8363.
[26] H. Manzano, J.S. Dolado, A. Ayuela, Elastic properties of the main species present in Portland cement pastes, Acta Mater. 57 (2009) 1666–1674.
[27] R. Dupuis, J.S. Dolado, J. Surga, A. Ayuela, Doping as a way to protect silicate chains in calcium silicate hydrates, ACS Sustain. Chem. Eng. 6 (2018) 15015–15021.
[28] Y. Du, Y. Zhu, S. Xi, P. Yang, H.O. Moser, M.B.H. Breese, A. Borgna, XAFCA: a new XAFS beamline for catalysis research, J. Synchrotron Radiat. 22 (2015) 839–843.
[29] B. Ravel, M. Newville, ATHENA, ARTEMIS, HEPHAESTUS: data analysis for X-ray absorption spectroscopy using IFEFFIT, J. Synchrotron Radiat. 12 (2005) 537–541.
[30] J. Mustre de Leon, J.J. Rehr, S.I. Zabinsky, R.C. Albers, Ab initio curved-wave x-ray-absorption fine structure, Phys. Rev. B 44 (1991) 4146–4156.
[31] M.D. Andersen, H.J. Jakobsen, J. Skibsted, Incorporation of aluminum in the calcium silicate hydrate (C−S−H) of hydrated Portland cements: a high-field ^{27}Al and ^{29}Si MAS NMR investigation, Inorg. Chem. 42 (2003) 2280–2287.

[32] M. Magi, E. Lippmaa, A. Samoson, G. Engelhardt, A.R. Grimmer, Solid-state high-resolution silicon-29 chemical shifts in silicates, J. Phys. Chem. 88 (1984) 1518–1522.
[33] M. Kunz, A.A. MacDowell, W.A. Caldwell, D. Cambie, R.S. Celestre, E.E. Domning, R.M. Duarte, A.E. Gleason, J.M. Glossinger, N. Kelez, D.W. Plate, T. Yu, J.M. Zaug, H.A. Padmore, R. Jeanloz, A.P. Alivisatos, S.M. Clark, A beamline for high-pressure studies at the advanced light source with a superconducting bending magnet as the source, J. Synchrotron Radiat. 12 (2005) 650–658.
[34] H.K. Mao, J. Xu, P.M. Bell, Calibration of the ruby pressure gauge to 800 kbar under quasi-hydrostatic conditions, J. Geophys. Res.-Solid Earth 91 (1986) 4673–4676.
[35] F. Birch, Finite strain isotherm and velocities for single-crystal and polycrystalline NaCl at high pressures and 300°K, J. Geophys. Res.-Solid Earth 83 (1978) 1257–1268.
[36] J.D. Gale, GULP: a computer program for the symmetry-adapted simulation of solids, J. Chem. Soc. Faraday Trans. 93 (1997) 629–637.
[37] S. Plimpton, Fast parallel algorithms for short-range molecular dynamics, J. Comput. Phys. 117 (1995) 1–19.
[38] A.C.T. van Duin, S. Dasgupta, F. Lorant, W.A. Goddard, ReaxFF: a reactive force field for hydrocarbons, J. Phys. Chem. A 105 (2001) 9396–9409.
[39] H. Manzano, R.J.M. Pellenq, F.-J. Ulm, M.J. Buehler, A.C.T. van Duin, Hydration of calcium oxide surface predicted by reactive force field molecular dynamics, Langmuir 28 (2012) 4187–4197.
[40] A.C.T. van Duin, A. Strachan, S. Stewman, Q. Zhang, X. Xu, W.A. Goddard, $ReaxFF_{SiO}$ reactive force field for silicon and silicon oxide systems, J. Phys. Chem. A 107 (2003) 3803–3811.
[41] K.L. Joshi, G. Psofogiannakis, A.C.T. van Duin, S. Raman, Reactive molecular simulations of protonation of water clusters and depletion of acidity in H-ZSM-5 zeolite, PCCP 16 (2014) 18433–18441.
[42] I.G. Richardson, Tobermorite/jennite- and tobermorite/calcium hydroxide-based models for the structure of C-S-H: applicability to hardened pastes of tricalcium silicate, β-dicalcium silicate, Portland cement, and blends of Portland cement with blast-furnace slag, metakaolin, or silica fume, Cem. Concr. Res. 34 (2004) 1733–1777.
[43] J. Moon, J.E. Oh, M. Balonis, F.P. Glasser, S.M. Clark, P.J.M. Monteiro, Pressure induced reactions amongst calcium aluminate hydrate phases, Cem. Concr. Res. 41 (2011) 571–578.
[44] X. Hou, R.J. Kirkpatrick, L.J. Struble, P.J.M. Monteiro, Structural investigations of alkali silicate gels, J. Am. Ceram. Soc. 88 (2005) 943–949.
[45] C.E. Tambelli, J.F. Schneider, N.P. Hasparyk, P.J.M. Monteiro, Study of the structure of alkali–silica reaction gel by high-resolution NMR spectroscopy, J. Non-Cryst. Solids 352 (2006) 3429–3436.
[46] A. Kunhi Mohamed, P. Moutzouri, P. Berruyer, B.J. Walder, J. Siramanont, M. Harris, M. Negroni, S.C. Galmarini, S.C. Parker, K.L. Scrivener, L. Emsley, P. Bowen, The atomic-level structure of cementitious calcium aluminate silicate hydrate, J. Am. Chem. Soc. 142 (2020) 11060–11071.
[47] T. Maeshima, H. Noma, M. Sakiyama, T. Mitsuda, Natural 1.1 and 1.4 nm tobermorites from Fuka, Okayama, Japan: chemical analysis, cell dimensions, 29Si NMR and thermal behavior, Cem. Concr. Res. 33 (2003) 1515–1523.
[48] K. Mohan, H.F.W. Taylor, A trimethylsilylation study of tricalcium silicate pastes, Cem. Concr. Res. 12 (1982) 25–31.
[49] A. Nonat, The structure and stoichiometry of C-S-H, Cem. Concr. Res. 34 (2004) 1521–1528.
[50] A. Ayuela, J.S. Dolado, I. Campillo, Y.R.D. Miguel, E. Erkizia, D. Sánchez-Portal, A. Rubio, A. Porro, P.M. Echenique, Silicate chain formation in the nanostructure of cement-based materials, J. Chem. Phys. 127 (2007) (164710).
[51] T. Mitsuda, H.F.W. Taylor, Normal and anomalous tobermorites, Mineral. Mag. 42 (1978) 229–235.
[52] M. Miyake, S. Komarneni, R. Roy, Kinetics, equilibria and thermodynamics of ion exchange in substituted tobermorites, Mater. Res. Bull. 24 (1989) 311–320.
[53] K. Sasaki, T. Masuda, H. Ishida, T. Mitsuda, Structural degradation of tobermorite during vibratory milling, J. Am. Ceram. Soc. 79 (1996) 1569–1574.
[54] I.G. Richardson, A.R. Brough, R. Brydson, G.W. Groves, C.M. Dobson, Location of aluminum in substituted calcium silicate hydrate (C-S-H) gels as determined by ^{29}Si and ^{27}Al NMR and EELS, J. Am. Ceram. Soc. 76 (1993) 2285–2288.
[55] H. Manzano, J.S. Dolado, A. Ayuela, Aluminum incorporation to dreierketten silicate chains, J. Phys. Chem. B 113 (2009) 2832–2839.
[56] M.J. Abdolhosseini Qomi, F.-J. Ulm, R.J.-M. Pellenq, Evidence on the dual nature of aluminum in the calcium-silicate-hydrates based on atomistic simulations, J. Am. Ceram. Soc. 95 (2012) 1128–1137.
[57] H. Manzano, J.S. Dolado, M. Griebel, J. Hamaekers, A molecular dynamics study of the aluminosilicate chains structure in Al-rich calcium silicate hydrated (C–S–H) gels, Phys. Status Solidi A 205 (2008) 1324–1329.
[58] E. Pavón, F.J. Osuna, M.D. Alba, L. Delevoye, Direct evidence of Lowenstein's rule violation in swelling high-charge micas, Chem. Commun. 50 (2014) 6984–6986.
[59] S.E. Dann, P.J. Mead, M.T. Weller, Löwenstein's rule extended to an aluminum rich framework. The structure of bicchulite, $Ca_8(Al_2SiO_6)4(OH)_8$, by MASNMR and neutron diffraction, Inorg. Chem. 35 (1996) 1427–1428.
[60] C.E. White, J.L. Provis, T. Proffen, D.P. Riley, J.S.J. van Deventer, Combining density functional theory (DFT) and pair distribution function (PDF) analysis to solve the structure of metastable materials: the case of metakaolin, PCCP 12 (2010) 3239–3245.
[61] T. Charpentier, K. Okhotnikov, A.N. Novikov, L. Hennet, H.E. Fischer, D. R. Neuville, P. Florian, Structure of strontium aluminosilicate glasses from molecular dynamics simulation, neutron diffraction, and nuclear magnetic resonance studies, J. Phys. Chem. B 122 (2018) 9567–9583.
[62] K. Okhotnikov, B. Stevensson, M. Edén, New interatomic potential parameters for molecular dynamics simulations of rare-earth (RE = La, Y, Lu, Sc) aluminosilicate glass structures: exploration of RE^{3+} field-strength effects, PCCP 15 (2013) 15041–15055.
[63] J. Li, W. Zhang, K. Garbev, G. Beuchle, P.J.M. Monteiro, Influences of cross-linking and Al incorporation on the intrinsic mechanical properties of tobermorite, Cem. Concr. Res. 136 (2020) 106170.
[64] F. Shimizu, S. Ogata, J. Li, Theory of shear banding in metallic glasses and molecular dynamics calculations, Mater. Trans. 48 (2007) 2923–2927.
[65] Q.Y. Hu, J.F. Shu, A. Cadien, Y. Meng, W.G. Yang, H.W. Sheng, H.K. Mao, Polymorphic phase transition mechanism of compressed coesite, Nat. Commun. 6 (2015) 6630.
[66] S.-N. Luo, T.J. Ahrens, P.D. Asimow, Polymorphism, superheating, and amorphization of silica upon shock wave loading and release, J. Geophys. Res.-Solid Earth 108 (2003) 2421.